RSC Advances

PAPER

View Article Online
View Journal | View Issue

Cite this: *RSC Adv.*, 2017, **7**, 22553

Monocrystalline NiS nanowire arrays supported by Ni foam as binder-free electrodes with outstanding performances†

Yali Xu,[ab] Weimin Du,[*a] Lulu Du,[ac] Wenjuan Zhu,[a] Wei Guo,[a] Jingjing Chang,[a] Bing Zhang[c] and Dehua Deng[a]

Received 2nd February 2017
Accepted 17th April 2017

DOI: 10.1039/c7ra01360d

rsc.li/rsc-advances

Monocrystalline NiS nanowire arrays supported by Ni foam were synthesized without any surfactant. Characterization results reveal that the as-obtained NiS nanowires belong to a rhombohedral phase with higher aspect ratio. Electrochemical measurements indicate these nanowire arrays can achieve a higher areal capacitance of 8.7 F cm^{-2} at the current density of 20 mA cm^{-2}, together with good rate capability and excellent cycling stability (78.7% capacitance retention after 8000 cycles).

Owing to crude oil depletion and global warming aggravation, there is an urgent need for effective means in energy storage and conversion to satisfy the demands of energy sources and environment in future. Thus, supercapacitors (SCs), also known as electrochemical capacitors, have aroused extensive interest due to their many merits, such as: high specific power density, long cycle life, and fast charge and discharge rates, *etc.*[1–6] However, the energy densities of SCs are usually lower than those of Li-ion batteries due to the restriction of limited charge storage in the surface (or near-surface) of electrodes.[7] How to effectively enhance the energy densities of SCs has become one of the current research focuses. According to the calculation equation: $E = C \times \Delta V^2/2$, E (energy density) is proportional to C (specific capacitance) and ΔV (potential window of discharge). Both higher specific capacitance and wider working voltage window will be beneficial to the increase of energy density.[8,9] Hence, seeking ideal electrode materials with higher specific capacitance is always the hot-point issue in the past decade.

Currently, metal sulfides have attracted more and more attentions because of the potential application in many fields, *e.g.*: Li-ion batteries, supercapacitors, solar cells, photo-catalysts and adsorption agent, *etc.*[10–14] Among the family of metal sulfides, Ni–S series of compounds seem to be the most appealing because they not only present many stoichiometric proportion, such as NiS, Ni_3S_2, Ni_4S_3, Ni_7S_6, and Ni_9S_8, but also exhibit the unique physical and chemical properties, including: metal insulation, better electrical conductivity, *etc.*[15–19] Besides, ordered nano-arrays are favorable to the electronic conduction along the axial direction, which can tremendously enhance the electrochemical performance in energy storage, especially for supercapacitors. Based on the above facts, the application of ordered nano-arrays in SCs has also ignited researchers' great interest.[20–23] Some Ni–S series of compound nano-arrays with different morphologies and compositions have been prepared and investigated the energy storage performance, *e.g.*: Ni_3S_2 nanowire arrays,[24] NiS nanotube arrays,[25] and NiS nanoplatelet arrays,[26] *etc.* But to the best of our knowledge, there are fewer reports about the synthesis and electrochemical performance of NiS nanowire arrays up to date. Thus, one can see that it is significant and challenging to exploit NiS nanowire arrays as supercapacitor electrodes. Simultaneously, it will largely enrich the species of electrode materials applicable for supercapacitors.

According to the above considerations, monocrystalline NiS nanowire arrays (NWAs) with higher aspect ratio were successfully grown on Ni foam by a facile one-step solvothermal approach, and then directly used as the electrodes of SCs. Detailed experimental procedures are provided in ESI.† Remarkably, these monocrystalline NiS NWAs manifested a higher areal capacitance of 8.7 F cm^{-2} at 20 mA cm^{-2}, together with good rate capability and excellent cycling stability.

The morphologies of the products supported by Ni foam are observed by Scanning Electron Microscope (SEM). Different magnification images are shown in Fig. 1. According to Fig. 1a,

[a]*Henan Province Key Laboratory of New Optoelectronic Functional Materials, College of Chemistry and Chemical Engineering, Anyang Normal University, Anyang, Henan, 455002, P. R. China. E-mail: dwmchem@163.com; Fax: +86-372-290-0213; Tel: +86-372-290-0040*

[b]*College of Chemistry and Molecular Engineering, Zhengzhou University, Zhengzhou, Henan, 450001, P. R. China*

[c]*School of Chemical Engineering and Energy, Zhengzhou University, Zhengzhou, Henan, 450001, China*

† Electronic supplementary information (ESI) available: Experimental details, XRD patterns of the NiS nanowire arrays supported by Ni foam, elemental mappings of Ni and S elements of NiS NWAs stripped from Ni foam, specific capacitance of NiS NWAs at different scanning rates, comparison of the electrochemical performances of the present NiS NWAs with previously reported Ni–S nanostructures and other representative nanomaterials. See DOI: 10.1039/c7ra01360d

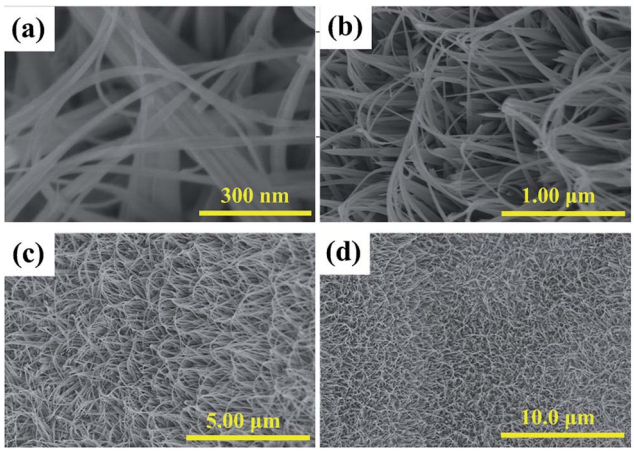

Fig. 1 Different magnification SEM images of the typical samples supported by Ni foam.

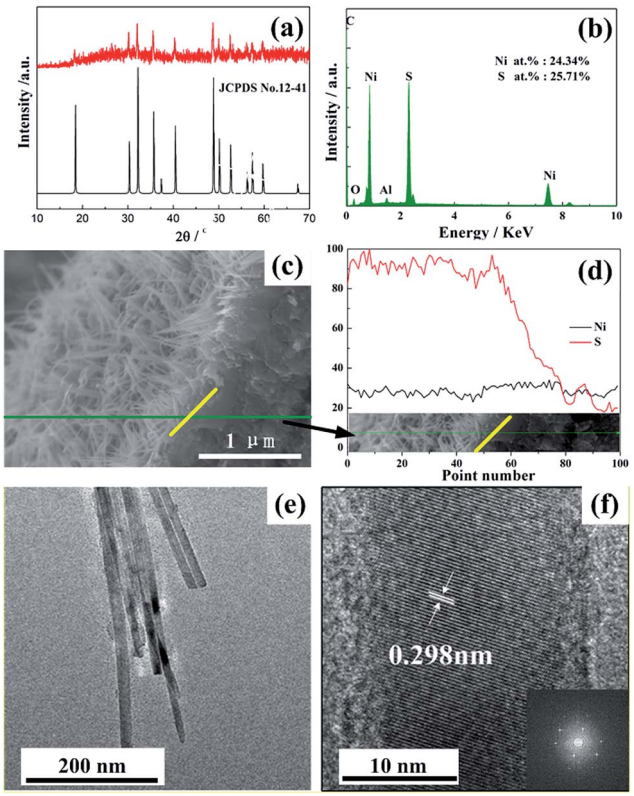

Fig. 2 (a) XRD pattern, (b) EDX microanalysis and corresponding elemental contents (the inset) of the products stripped from Ni foam; (c) cross section image of NiS nanowires arrays; (d) line scanning EDX analysis; (e) TEM image; (f) HRTEM image and the corresponding FFT pattern (the inset) of NiS NWAs stripped from Ni foam.

the as-obtained products take on the uniform wire-like shapes. After careful observation and calculation, the diameter of the single nanowire is about 30 nm. But some thick wire-like materials also appear in the visible region. It can be ascribed to the aggregation of several nanowires. From the lower magnification image in Fig. 1b, it can be seen that the length of these nanowires is about 2 μm. These uniformly nanowires can achieve a higher aspect ratio of 67 : 1. Meanwhile, they form a interconnecting 3D nanostructure due to the longer length. As shown in Fig. 1c, these nanowires with higher aspect ratio made up ordered nano-arrays just like the reed rolling. These 3D nanowire arrays supported by Ni foam can be synthesized in larger scale through the presented solvothermal approach (Fig. 1d). This unique structure provides a 3D interconnected network of both electron and ions pathways, which can facilitate efficient charge and mass exchange during faradaic redox reactions, implying the promising applied values in supercapacitors.[27]

The crystalline structure and the composition of the stripped products from Ni foam were characterized by X-ray diffraction (XRD) and energy-dispersive X-ray analysis (EDX), respectively. The typical peaks of samples display a rhombohedral phase of NiS (ICPDS no. 12-41) with *R3m* space group. NiS nano-arrays supported by Ni foam were also measured and corresponding XRD patterns are provided in ESI Fig. S1.† The stronger signs were ascribed to the peaks of the Ni foam. Due to the thinner layer of NiS NWAs, the intensity of Ni foam peaks is more intense than those of NiS NWAs. In order to further confirm the formation of NiS nanowires, EDX was carried out. Results demonstrated that the synthesized samples only contain the elements of Ni, S, Al, C and O without any other impure energy peaks (Fig. 2b). The element of C is from the conductive adhesive. Al and O are from the sample holder. From the EDX data inserted in Fig. 2b, the mole ratio of Ni and S atoms is 1 : 1.06, agreeing well with its stoichiometric proportion. In addition, all elements are uniformly distributed in NiS NWAs according to the element mapping images (Fig. S2†). It adequately manifests that Ni and S atoms could be well distributed in the as-prepared NiS NWAs. The cross-section image of NiS NWAs in Fig. 2c reveals the thickness of the NiS nanowire arrays is around 1 μm, showing a higher loading amount of the electroactive material. Due to the bending of nanowires, the longest length of NiS nanowires can achieve to 2 μm which is consistent with Fig. 1. The relative changing trend of the elemental contents are shown in Fig. 2d. The red line (see Fig. 2d) is the content of elemental sulfur. On the right of the yellow line, the sulfur content is falling rapidly. So, the yellow line is the boundary of NiS nanoarrays and Ni foam substrate. Transmission Electron Microscopy (TEM) image in Fig. 2e shows a 2D projection picture of 3D NiS nanowire. Clear lattice fringes shown in high-resolution TEM image (Fig. 2f) are visible which proves the monocrystalline structure. The interplane distance of 0.298 nm corresponds to (101) plane of rhombohedral phase NiS. Besides, a fast Fourier transform pattern is provided in the inset of Fig. 2f. Hexagonal spots again demonstrate the rhombohedral phase of NiS nanowires.

To evaluate the potential application of NiS NWAs as high-performance electrode of SCs, cyclic voltammogram (CV), galvanostatic charge–discharge (GCD), cyclic stability and electrochemical impedance spectroscopy (EIS) were tested. The nominal area of NiS NWAs immersed in 3 mol dm^{-3} KOH electrolyte is controlled as about 1 cm^2. Based on the quality

change of Ni foam before and after the reaction, the loaded amount of monocrystalline NiS nanowires were calculated as 6.0 mg cm^{-2} (or 60 mg cm^{-3}). Electrochemical properties were tested in a three-electrode cell with a standard calomel electrode (SCE) as the reference electrode and a platinum electrode as counter electrode. Detailed measurement process and the calculating methods of areal/specific capacitance can be found in ESI.† Fig. 3a shows the CV curves at various scanning rates. Apparently, a pair of symmetrical redox peaks is observed in every CV curve within the potential range from −0.2 to 0.6 V, which belongs to the faradaic redox reaction between Ni^{2+}/Ni^{3+} and OH^- in KOH electrolyte, as shown below:[28]

$$NiS + OH^- \rightarrow NiSOH + e^-$$

Moreover, the increase of scanning rate can lead to the shift of redox peaks positions, which results from the strengthening electric polarization during the charge/discharge process. When the scanning rate increased to 20 mV s^{-1}, the anode peak disappeared, indicating that the NiS NWAs prefer to exhibit electrochemical capacitance property. Further, the CVs get some distort with the increased scanning rate due to the low conductance of transition metal compounds. Based on the eqn (S1) in ESI,†[29] the specific capacitances (C_{sp}) of the NiS NWAs were calculated to be 2187.5, 1945.8, 1767.8, 1595.8 and 1034.4 F g^{-1} at 3, 5, 7, 10 and 20 mV s^{-1}, respectively (see ESI Fig. S1†). This phenomenon can be attributed to the diffusion effect limiting the diffusion and migration of the electrolyte ions within the electrode.[30]

The GCD tests were accomplished between −0.2 and 0.4 V (*vs.* SCE) and the experimental results were shown in Fig. 3b. Obviously, there is a distinct voltage plateau region in every potential–time curve, which re-confirms the faradaic redox pseudocapacitance.[31,32] Nevertheless, the plateau gets shorter and more declining when the current densities increased to 50 mA cm^{-2}. It indicates that NiS NWAs have battery feature at lower discharging current density and electrochemical capacitance properties at higher discharging current density.[33] The areal/mass specific capacitances can be calculated according to eqn (S2) and (S3) in ESI.†[29] The corresponding areal/mass specific capacitances can be calculated as 8.7, 8.0, 6.6, 6.1, 5.5 F cm^{-2} and 1456.7, 1333.3, 1108.3, 1023.3, 920.0 F g^{-1} at the current densities of 20, 25, 35, 40 and 50 mA cm^{-2}, respectively (Fig. 3c). With the increase of current densities, specific capacitance is gradually decreased. It can be attributed to the fact that a portion of materials are insufficient involved in the redox reaction at higher current densities.[34,35] The capacitance retention for NiS NWAs is 63.2% when the current density is increased to 50 mA cm^{-2}, which indicates better rate capability. For Ni–S series of compounds, such higher areal/mass specific capacitances are rarely reported. Comparison of electrochemical performances of the present NiS NWAs and previously reported NiS nanostructures is shown in Fig. 3d. Detailed information of NiS nanostructures and the source references were listed in ESI Table S1.† Generally, the specific capacitance of electrodes will increase along with the decrease of current densities. Therefore, the specific capacitances at lower current density were selected as far as possible for comparison in the published article. But as for ref. S2 and S4† (see ESI Table S1†), the capacitances at smaller current densities are not fond in the literatures. As a result, the present NiS NWAs supported by Ni foam display higher specific capacitance compared with previously reported NiS nanostructures except the ref. S11.† Comparison of NiS NWAs with the reported other nanomaterials was presented in ESI Table S2.† Clearly, these NiS NWAs exhibit a much higher specific capacitance than other metal compound nanostructures. Therefore, ordered NiS NWAs supported by Ni foam possess higher specific capacitances and good rate capability.

Long-time cycling performance of NiS NWAs is presented in Fig. 4a. During the whole 8000 cycles, specific capacitance drops gradually which could be ascribed to the reciprocal phase exchange between NiS and NiSOH during the charge–discharge process, which results in part collapse of NiS NWAs.[36] Remarkably, *ca.* 78.7% of the initial capacitance can still be kept even after 8000 cycles. The first and the last ten charge–discharge curves were inserted in Fig. 4a. It can be seen that the shapes of these GCD curves remain almost unchanged indicating better electrode reversibility. These results evidently suggest the great promise of NiS NWAs for high-performance SCs characterized by both higher specific capacitances and long cycle stability. To

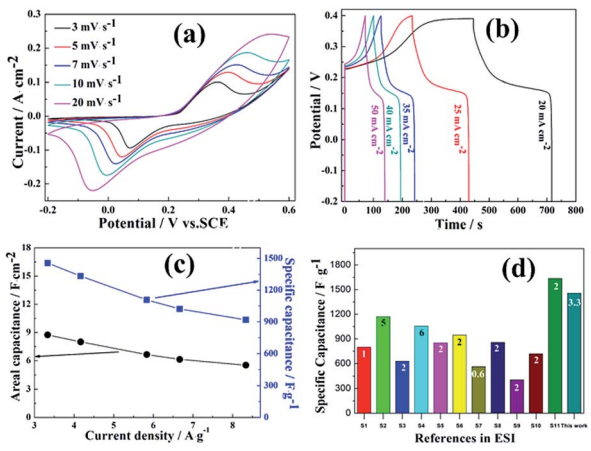

Fig. 3 (a) CV curves at various scanning rates ranging from 3 to 20 mV s^{-1}; (b) GCD curves at different current density; (c) specific capacitance and areal capacitance at different current density, and (d) comparison of electrochemical performances of the present NiS NWAs with previously reported NiS nanostructures (the *X*-axis shows reference number which correspond to the references in ESI Table S1,† the numbers in the coloured bars represent the current densities).

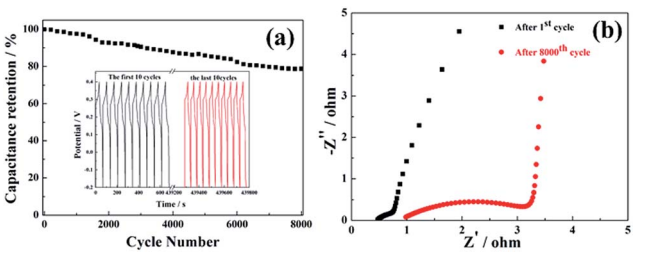

Fig. 4 (a) Cycling performances of NiS NWAs at 50 mA cm^{-2} (b) EIS plot of the NiS NWAs after the 1st and the 8000th cycles.

identify the enhanced electrical conductivity of NiS NWAs, the electrochemical impedance spectroscope (EIS) was measured at a frequent from 0.01 Hz to 100 kHz. The EIS plots of the NiS NWAs after the 1st and the 8000th cycles are shown in Fig. 4b. Both of them can be represented as a two-part Nyquist graph: a semicircle at high frequency revealing the charge transfer resistance (R_{ct}) which caused by faradic reactions and double-layer capacitance on the surface of materials; a straight line at low frequency showing the capacitive behavior. The intersection of the semicircle with the real axis represents R_{ct}. The R_{ct} values after the 1st and the 8000th cycles are tested to be 0.47 Ω and 0.98 Ω. The smaller R_{ct} of NiS NWAs demonstrates favorable diffusion of ion and electron transport.[37] The increase of R_{ct} value after 8000 cycles could be attributed to the part collapse of NiS NWAs which is reflected in the gradual reduction of the specific capacitance during 8000 cycles. Taking into account the structural features of NiS NWAs, the reason why this electrode material has these advantages can be listed as follows: firstly, the ordered NiS NWAs are a porous open structure, which is beneficial for the penetration of electrolyte to electrode and shortening the diffusion path of ions. Meanwhile, the open space can serve as a powerful ion storage layer to ensure reaction to continue. Secondly, NiS NWAs can provide an efficient way to store and transport electrons and charge. Thirdly, the direct contact between the conductive substrate and each NiS nanowires avoids the use of polymer binder or conductive agent, greatly reducing the "dead zone" of the electrodes. All in all, ordered NiS NWAs supported by Ni foam will be an excellent candidate in the field of energy storage in the future.

In summary, a facile solvothermal method was used to synthesis monocrystalline NiS NWAs with a diameter of 30 nm and a length of 2 μm. The unique 3D NiS NWAs are endowed with fast ion and electron transport, favorable infiltration of electrolyte solution and more electrochemical active sites. The excellent electrochemical performance were achieved for the ordered NiS NWAs supported by Ni foam, such as: higher capacitance, better rate capability and excellent cycle stability. These outstanding results demonstrate ordered NiS NWAs are highly hopeful for application in supercapacitor devices.

Acknowledgements

The authors gratefully acknowledge the financial support from the National Natural Science Foundation of China (U1404203), Plan For Scientific Innovation Talent of Henan Province (174200510017), Program for Innovative Research Team of Science and Technology in the University of Henan Province (16IRTSTHN003), National Students' Innovation and Entrepreneurship Training Program of China (201410479011, 201510479009) and, Special projects of new energy vehicle development of Anyang City.

Notes and references

1 P. J. Hall, M. Mirzaeian, S. I. Fletcher, F. B. Sillars, A. J. R. Rennie, G. O. Shittabey, G. Wilson, A. Cruden and R. Carter, *Energy Environ. Sci.*, 2010, **3**, 1238–1251.
2 P. Simon and Y. Gogotsi, *Nat. Mater.*, 2008, **7**, 845–854.
3 G. Wang, L. Zhang and J. Zhang, *Chem. Soc. Rev.*, 2012, **41**, 797–828.
4 A. Al-Osta, V. V. Jadhav, M. K. Zate, R. S. Mane, K. N. Hui and S.-H. Han, *Scr. Mater.*, 2015, **99**, 29–32.
5 X. Wang, Y. Chen, O. G. Schmidt and C. Yan, *Chem. Soc. Rev.*, 2016, **45**, 1308–1330.
6 T. Yang, T. Qian, M. Wang, X. Shen, N. Xu, Z. Sun and C. Yan, *Adv. Mater.*, 2016, **28**, 539–545.
7 Y. Wang, Y. Song and Y. Xia, *Chem. Soc. Rev.*, 2016, **45**, 5925–5950.
8 L. Demarconnay, E. Raymundo-Piñero and F. Béguin, *J. Power Sources*, 2011, **196**, 580–586.
9 W. G. Pell and B. E. Conway, *J. Power Sources*, 2004, **136**, 334–345.
10 H. Ruan, Y. Li, H. Qiu and M. Wei, *J. Alloys Compd.*, 2014, **588**, 357–360.
11 C. Sun, M. Ma, J. Yang, Y. Zhang, P. Chen, W. Huang and X. Dong, *Sci. Rep.*, 2014, **4**, 7054–7059.
12 C. V. V. M. Gopi, S. S. Rao, S. K. Kim, D. Punnoose and H. J. Kim, *J. Power Sources*, 2015, **275**, 547–556.
13 J. Zhang, L. Qi, J. Ran, J. Yu and S. Z. Qiao, *Adv. Eng. Mater.*, 2014, **4**, 716–723.
14 M. Ghaedi, M. Pakniat, Z. Mahmoudi, S. Hajati, R. Sahraei and A. Daneshfar, *Spectrochim. Acta, Part A*, 2014, **123**, 402–409.
15 J. T. Sparks and T. Komoto, *Rev. Mod. Phys.*, 1968, **40**, 752–754.
16 A. Manthiram and Y. U. Jeong, *J. Solid State Chem.*, 1999, **147**, 679–681.
17 R. Akbarzadeh, H. Dehghani and F. Behnoudnia, *Dalton Trans.*, 2014, **43**, 16745–16753.
18 C. H. Lai, K. W. Huang, J. H. Cheng, C. Y. Lee, W. F. Lee, C. T. Huang, B. J. Hwang and L. J. Chen, *J. Mater. Chem.*, 2009, **19**, 7277–7283.
19 J. Wang, S. Y. Chew, D. Wexler, G. X. Wang, S. H. Ng, S. Zhong and H. K. Liu, *Electrochem. Commun.*, 2007, **9**, 1877–1880.
20 G. Q. Zhang, H. B. Wu, H. E. Hoster, M. B. Chan-Park and X. W. Lou, *Energy Environ. Sci.*, 2012, **5**, 9453–9456.
21 S. E. Moosavifard, S. Fani and M. Rahmanian, *Chem. Commun.*, 2016, **52**, 4517–4520.
22 D. P. Dubal, G. S. Gund, C. D. Lokhande and R. Holze, *Energy Technol.*, 2014, **2**, 401–408.
23 J. Xu, Q. Wang, X. Wang, Q. Xiang, B. Liang, D. Chen and G. Shen, *ACS Nano*, 2013, **7**, 5453–5462.
24 C.-H. Lai, K.-W. Huang, J.-H. Cheng, C.-Y. Lee, W.-F. Lee, C.-T. Huang, B.-J. Hwang and L.-J. Chen, *J. Mater. Chem.*, 2009, **19**, 7277–7283.
25 Y. Li, Y. Chang, Y. Zhao, J. Wang and C. W. Wang, *J. Alloys Compd.*, 2016, **679**, 384–390.
26 W. Zhao, X. Zhu, H. Bi, H. Cui, S. Sun and F. Huang, *J. Power Sources*, 2013, **242**, 28–32.
27 J. Wang, Q. Zhang, X. Li, D. Xu, Z. Wang, H. Guo and K. Zhang, *Nano Energy*, 2014, **6**, 19–26.
28 Z. Li, A. Gu, J. Sun and Q. Zhou, *New J. Chem.*, 2016, **40**, 1663–1670.

29 J. H. Kim, Y. S. Lee, A. K. Sharma and C. G. Liu, *Electrochim. Acta*, 2006, **52**, 1727–1732.
30 J. Yan, Z. J. Fan, W. Sun, G. Q. Ning, T. Wei, Q. Zhang, R. F. Zhang, L. J. Zhi and F. Wei, *Adv. Funct. Mater.*, 2012, **22**, 2632–2641.
31 H. Jiang, T. Zhao, C. Li and J. Ma, *J. Mater. Chem.*, 2011, **21**, 3818–3823.
32 Z. Xing, Q. Chu, X. Ren, J. Tian, A. M. Asiri, K. A. Alamry, A. O. Al-Youbi and X. Sun, *Electrochem. Commun.*, 2013, **32**, 9–13.
33 D. Zhang, X. Zhou, K. Ye, Y. Li, C. Song, K. Cheng, D. Cao, G. Wang and Q. Li, *Electrochim. Acta*, 2015, **173**, 209–214.
34 D. Guo, P. Zhang, H. Zhang, X. Yu, J. Zhu, Q. Li and T. Wang, *J. Mater. Chem. A*, 2013, **1**, 9024–9027.
35 S. K. Meher, P. Justin and G. R. Rao, *Electrochim. Acta*, 2010, **55**, 8388–8396.
36 J. Yang, X. Duan, Q. Qin and W. Zheng, *J Mater Chem A*, 2013, **1**, 7880–7884.
37 K. Qiu, Y. Lu, D. Zhang, J. Cheng, H. Yan, J. Xu, X. Liu, J. K. Kim and Y. Luo, *Nano Energy*, 2015, **11**, 687–696.